Hindawi
Journal of Nanomaterials
Volume 2018, Article ID 8457670, 13 pages
https://doi.org/10.1155/2018/8457670

*Research Article*

# Effect of Nano-ppy/OMMT on the Physical and Electrochemical Properties of an Ionic Liquid Gel Polymer Electrolyte

**Shuo Yang, Xuan Li, and Pei Yao**

*School of Materials Science and Engineering, Tianjin University, Tianjin 300072, China*

Correspondence should be addressed to Xuan Li; lixuan412@tju.edu.cn and Pei Yao; pyaotju@163.com

Received 19 October 2017; Accepted 23 November 2017; Published 24 January 2018

Academic Editor: Ester Vazquez



A new type of nanopolypyrrole/organically modified montmorillonite-ionic liquid gel polymer electrolyte (ppy/OMMT-ILGPE) is prepared based on nanopolypyrrole/organically modified montmorillonite (ppy/OMMT), N-butyl-N- methylpyrrolidinium bis(trifluoromethanesulfonyl)imide (PP14TFSI), lithium-bis(trifluoromethanesulfonyl) (LiTFSI), polyvinylidene difluoride (PVDF), methyl methacrylate (MMA), and benzoyl peroxide (BPO) by an in situ method. The effect of nano-ppy/OMMT on the physical and electrochemical properties of an ionic liquid gel polymer electrolyte is demonstrated. The results show that nano-ppy/OMMT-ILGPE has a porous structure with a large surface area, and the diameter of the pores on the surface is approximately 1-2 $\mu$m. The $Li^+$ transference number of 0.72 is achieved, and the ionic conductivity reaches up to $1.2 \times 10^{-3}$ S/cm at room temperature. Nano-ppy/OMMT-ILGPE has good thermal stability and mechanical properties. Meanwhile, nano-ppy/OMMT-ILGPE has fine cycle performance in the Li|nano-ppy/OMMT-ILGPE|$LiNi_{1/3}Co_{1/3}Mn_{1/3}O_2$ coin cell. The good electrochemistry performance of nano-ppy/OMMT-ILGPE means that it can act as an ideal gel polymer electrolyte material for lithium ion batteries.

## 1. Introduction

The organic electrolyte plays an important part in lithium ion batteries (LIBs). However, the organic electrolyte is volatile, toxic, and explosive to the environment, and the development of LIBs has been limited. Therefore, ionic liquid gel polymer electrolytes (ILGPEs) that do not leak and have good electrochemical stability as well as high conductivity have increasingly drawn the attention of researchers in recent years [1–4]. With respect to ILGPEs, ionic liquids have more advantages than other liquid electrolytes, such as a higher dielectric constant, no combustibility, higher thermal stability, and less volatility [5]. PVDF, which has a high degree of crystallization, is a common organic polymer support material in the field of ILGPEs [6]. However, the high degree of crystallization may hinder the migration of lithium ions and increase the internal resistance of the LIB [7–9]. Polymethyl methacrylate (PMMA) also serves as a common organic polymer support material. PMMA with liquid electrolyte can form gel phases. Thus, the PMMA support material can adhere to the electrode and has a high ionic conductivity with liquid electrode well [10, 11]. However, the crystallization of PMMA is reduced after adding a liquid electrolyte, affecting the mechanical strength of PMMA [9, 10].

To improve the mechanical strength and electrochemical properties of the gel polymer electrolyte, nanolayered silicates are added to the gel polymer electrolyte and are called nanocomposites. Nanocomposites that have functional advantages and structures have a more promising future than other conventional gel polymer materials [11]. Among the commonly used inorganic layered structures, nanomontmorillonite (MMT) has been preferentially considered due to its special features, such as its length scale (clay channel width = $16 \times 10^{-10}$ m), high cation-exchange capacity (CEC ~ 80 mequiv./100 g), high aspect ratio (~1000), large specific surface area (~31.82 $m^2$/g), and appropriate interlayer charge (~0.55), which makes MMT suitable for nanocomposites [12]. During charge/discharge processes, the interaction between MMT and impurities from the polymer electrolyte and electrode improves the interfacial stability of the electrode and electrolyte [13, 14]. The high cationic

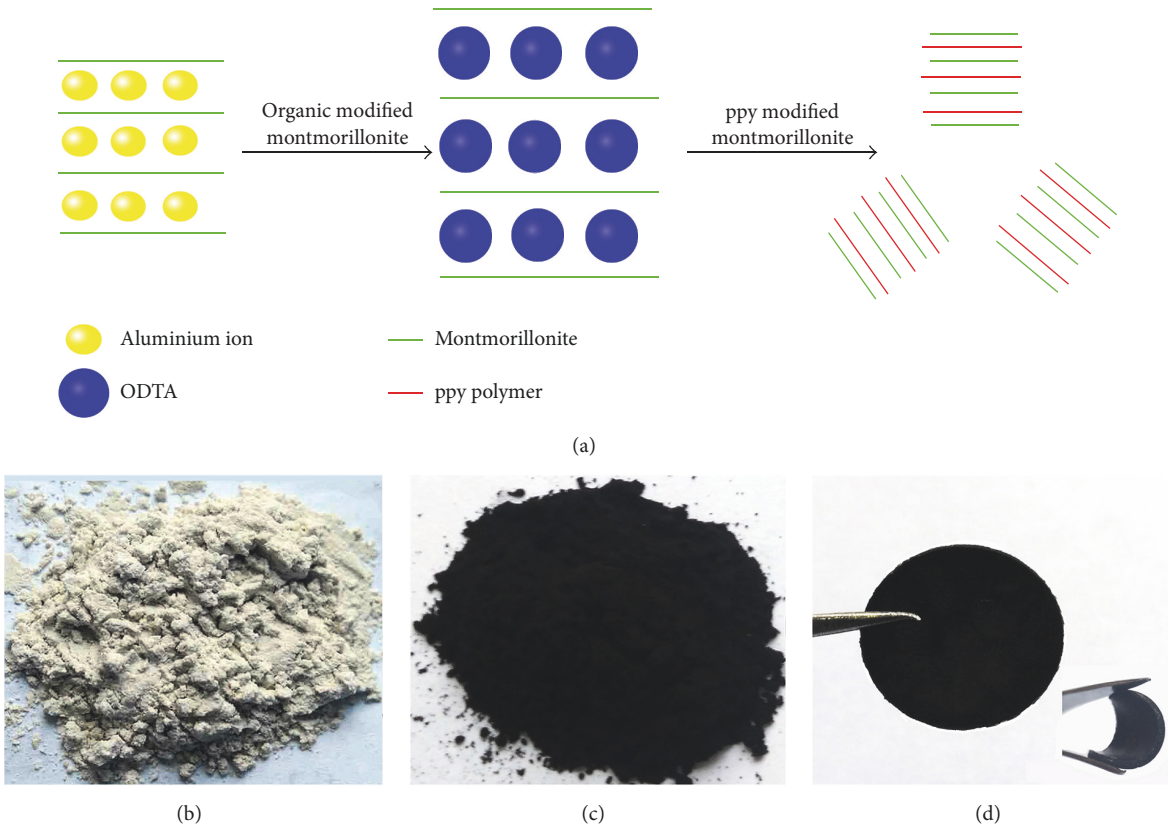


Figure 1: (a) Schematical representation of the preparation process of nano-ppy/OMMT, (b) MMT, (c) nano-ppy/OMMT, (d) nano-ppy/OMMT-ILGPE.

exchanges of MMT that act as Lewis acid centres on the surface can retard the transformation of cation and polymer segments into complexes [13], leading to changes of the MMT structure and the formation of conduction pathways. The interaction between the liquid electrolyte and MMT changes the micropore diameter of the polymer, enhancing the mechanical strength and absorbency rate of the liquid electrolyte [15, 16]. Thus, nano-MMT doped into an ILGPE would be beneficial to enhance the mechanical strength and electrochemical properties of the ILGPE.

In this work, under the action of $FeCl_3$ as the oxidant and sodium p-toluene sulfonate (TSANa) as the swelling agent, pyrrole (py) monomer was polymerized between the molecular layers of nano-organic modified montmorillonite (OMMT) by an in situ method. This method was used to prepare nano-ppy/OMMT, leading to enhanced electrochemical properties. Nano-ppy/OMMT was added to a homogenous solution (PVDF, MMA, BPO, LiTFSI, and PP14TFSI) at different ratios. Composite ionic liquid gel polymer electrolytes were prepared by this in situ method. A PVDF-PMMA copolymer was used as the support material for the ILGPE to reduce the crystallinity and improve the ionic conductivity. The PMMA amorphous phase absorbed the liquid electrolyte. The PVDF crystalline phase improved the mechanical capacity of the gel polymer electrolyte membrane. The microstructure and electrochemical performance of nano-ppy/OMMT-ILGPE are discussed in detail.

## 2. Experimental

*2.1. Modified Principle and Preparation of Nano-ppy/OMMT.* OMMT is prepared by the cationic exchange reaction between octadecyl dimethyl ammonium chloride (ODAC, AR, Tianjin Guangfu), as an organic intercalation agent, and $Al^{3+}$ in nano-MMT (AR, Aladdin). The grain diameter of nano-OMMT became smaller and the layer spacing expanded. This enhanced the access of py monomer (AR, Beijing J&K) to the space between the molecular layers. To further expand the OMMT layer spacing, py monomer was polymerized between the molecular layers during the reaction with $FeCl_3$ (AR, Tianjin Guangfu), as the oxidant, and TSANa (AR, Tianjin Guangfu), as the swelling agent. This method has been applied to prepare nano-ppy/OMMT, as shown in Figure 1(a) [15, 17, 18].

First, MMT was dissolved and stirred vigorously in deionized water for 12 h at 60°C until it was fully dispersed. Then, ODAC, an intercalating agent, was added (MMT and ODAC at a ratio of 5 : 1 by mass) and stirred for 15 h at 60°C until a homogenous solution was formed. Second, the solution TSANa and py monomer were mixed at the appropriate ratio and were dissolved and vigorously stirred

for 1 h at room temperature. Thirty millilitres of 1 mol/L $FeCl_3$ was added and stirred for 6 h at room temperature. Finally, the product was washed, separated by a centrifuge, and then placed into a high vacuum drying oven for 15 h at 80°C (see Figures 1(b) and 1(c)).

*2.2. The Preparation of Nano-ppy/OMMT-ILGPE.* PVDF (Aladdin Chemistry Co., Ltd.) was dissolved in N-methylpyrrolidone (NMP AR, Tianjin Guangfu) at a mass ratio of 1 : 8 and was stirred vigorously for 4 h. PP14TFSI (AR, Beijing HWRK Chemistry Co., Ltd., ionic liquid), LiTFSI (AR, Beijing J&K), MMA (AR, Tianjin Guangfu), and BPO (AR, Aladdin Chemistry Co. Ltd), at a mass fraction of 1.0 wt.% as an initiator, were added at the appropriate ratio (PVDF : PP14TFSI : LiTFSI : MMA = 1 : 1 : 1 : 1 (mass ratio)), and the mixture was stirred for 6 h until it became transparent and a homogenous solution formed. Nano-ppy/OMMT was added to the solution (its mass ratios with PVDF were 0.04 : 1, 0.06 : 1, 0.08 : 1, and 0.1 : 1). The mixture was continuously stirred for 12 h until a homogenous solution formed. The above process was performed at room temperature, and, then, the solution was heated in vacuum oven at 80°C for 10 h. This method was applied to prepare nano-ppy/OMMT-ILGPE (see Figure 1(d)) [19–21].

*2.3. Electrode Preparation and Cell Assembly.* The positive electrode was prepared by adding a $LiNi_{1/3}Co_{1/3}Mn_{1/3}O_2$ (Shenzhen KeJing Co., Ltd.) active material powder, acetylene black (Shenzhen KeJing Co., Ltd.), and PVDF binder at a mass ratio of 8 : 1 : 1 to NMP with constant stirring for 10 h at 100°C until a viscous slurry formed. Then, the resulting viscous slurry was cast onto an aluminium foil (14 mm thickness), as a current collector, and dried at 100°C in a vacuum oven for 10 h. A cell was assembled by sandwiching nano-ppy/OMMT-ILGPE between the $LiNi_{1/3}Co_{1/3}Mn_{1/3}O_2$ positive electrode and lithium metal negative electrode. Then, the cell was pressed with a hydraulic press at a pressure of 10 MPa. All of the manufactured cells were manufactured in a dry argon atmosphere glove box.

*2.4. Characterization.* IR spectra were effective at describing the characteristics and interactions of different groups. These were recorded in the spectral range of 4000 to 400 $cm^{-1}$ at room temperature. The chemical structures of MMT and nano-ppy/OMMT were investigated using the IR spectrometer (FTIR-1500) and Raman spectrometer (RENISHAW-inVia reflex). The interlayer spacing and crystallization of MMT, OMMT, and nano-ppy/OMMT were studied by X-ray diffraction (XRD) using an automatic Japanese D/MAX-2500 powder diffractometer with monochromatic Cu K$\alpha$ radiation under the following conditions: voltage and current of 30 kV and 30 mA, respectively; scanning range of $1^\circ \le 2\theta \le 15^\circ$; scanning speed of 3°/min; and incident X-ray wavelength of 0.154 nm. Scanning electron microscopy (SEM, Nano SEM 430) and transmission electron microscopy (TEM, JEM-2100F) were used to study the structure and surface morphology of MMT, nano-ppy/OMMT, ILGPE, and nano-ppy/OMMT-ILGPE. The tensile properties of ILGPE and nano-ppy/OMMT-ILGPE were evaluated at room temperature following ASTM D 638 type V method, using the universal material testing machine (WDW5000). The crosshead speed is 10 mm/min and the load cell capacity is 5000 N. For two specimens (10 mm × 5 mm), the measurements were taken and the values of tensile strength were calculated [22]. Thermogravimetric analysis (TGA, STA409EP, Netzsch) was performed to investigate the thermal characteristics of ILGPE and nano-ppy/OMMT-ILGPE from room temperature to 700°C at a heating rate of 10°C/min in a nitrogen atmosphere. AC impedance spectroscopy was used to test ionic conductivity of ILGPE and nano-ppy/OMMT-ILGPE with two stainless steel blocking electrodes over a frequency range from 0.01 Hz to $10^5$ Hz at 20°C. Both the Li-ion transference number determination and cyclic voltammetry (CV) were important in evaluating the performance of the electrolyte membrane. A combination of the amperometric *I-t* curve and AC impedance was applied to determine the Li-ion transference number. CV was used to measure the range of oxidation potential and reduction potential in the reversible electrode reaction. Electrochemical impedance spectroscopy (EIS) was used to investigate the interfacial behavior of the cells over a frequency range of 0.01 Hz to $10^5$ Hz with an amplitude of 10 mV. The above experiments were used with CHI660E. The charge/discharge performances and cycling behavior of the Li|nano-ppy/OMMT-ILGPE|$LiNi_{1/3}Co_{1/3}Mn_{1/3}O_2$ and Li|ILGPE|$LiNi_{1/3}Co_{1/3}Mn_{1/3}O_2$ cells were tested by battery testing equipment (CT2001A) with a testing voltage between 2.7 V and 4.2 V.

## 3. Results and Discussion

In Figure 2(a), 1020.98 and 1026.07 $cm^{-1}$ represent the vibration absorption of Si-O; 472.09 and 469.31 $cm^{-1}$ represent the bending vibration of O-Al in the MMT lattice. The polymerization reaction of the py monomer (Figure S1) between the layers of MMT has a small effect on the vibration absorption peaks. This indicates that the structure of MMT cannot be changed after organic modification [23]. ppy has the characteristic peaks of N-H and C=C. The vibration absorptions of N-H appear at 3460.22 and 1460.12 $cm^{-1}$, and the stretch vibration of C=C appears at 1640.23 $cm^{-1}$. This suggests that py monomer becomes ppy between the MMT layers.

Figure 2(b) shows the obvious differences of the MMT and nano-ppy/OMMT samples in the Raman spectra, which confirm the organic modification of the MMT. The several characteristic peaks at 1156, 1577, and 971 $cm^{-1}$ are ascribed to ring-stretching mode in the curve of nano-ppy/OMMT. They corresponded to the D-band (C-C, the disordered graphite structure), G-band (C=C, $sp^2$-hybridized carbon), and C-H in-plane deformation of ppy, respectively [24, 25]. It is in line with the result of FTIR (Figure 2(a)).

The interlayer spacing is calculated by using the following Bragg equation:

$$d = \frac{\lambda}{2 \sin \theta}, \quad (1)$$

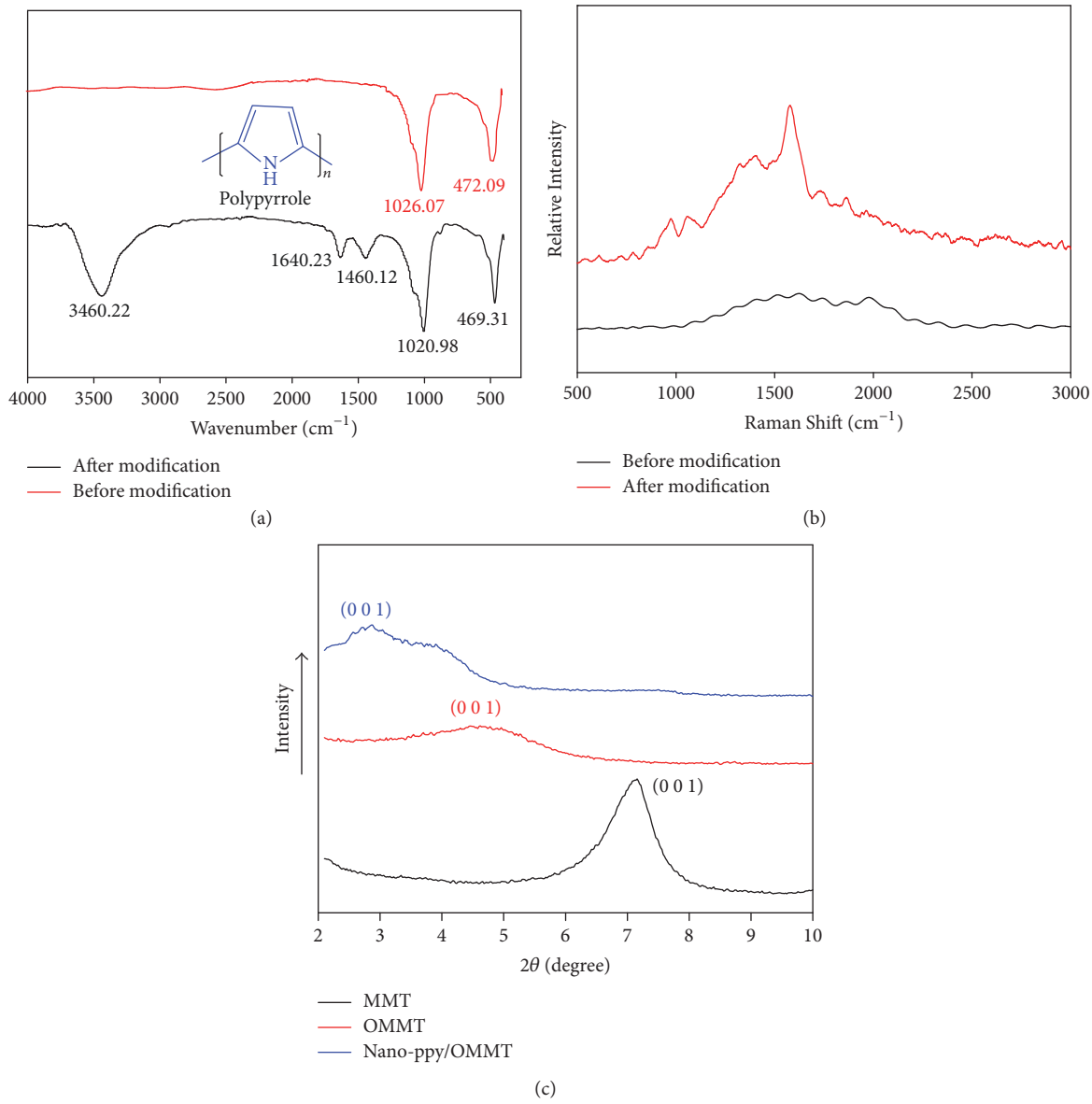


FIGURE 2: (a) IR spectrum of MMT and nano-ppy/PMMT. (b) Raman spectrum of MMT and nano-ppy/PMMT. (c) XRD profile of MMT, OMMT, and nano-ppy/OMMT.

where $d$ is the layer spacing, $\theta$ is the semi-diffraction angle, and $\lambda$ is the incident X-ray wavelength.

Figure 2(c) shows the XRD patterns of MMT, OMMT, and nano-ppy/OMMT. MMT exhibits the $(0\ 0\ 1)$ diffraction peak at $2\theta = 6.18^{\circ}$, corresponding to an interlayer spacing of 1.42 nm. The $(0\ 0\ 1)$ diffraction reflection shifts to $2\theta = 4.78^{\circ}$ for OMMT and corresponds to an interlayer spacing of 1.84 nm. This can be explained by the cationic exchange reaction between ODAC and MMT. The long alkyl chain of ODAC can increase the interlayer spacing of OMMT by up to 1.84 nm. The shape of the OMMT peak is broader, meaning that the crystallization of OMMT is weakened. Thus, it is easier for the py monomer to gain access between the layers of OMMT. Via interactions with $FeCl_3$, as the oxidant, and TSANa, as the swelling agent, py monomer undergoes the polymerization reaction in situ between the molecular layers. For nano-ppy/OMMT, the $(0\ 0\ 1)$ diffraction reflection shifts to $2\theta = 2.68^{\circ}$, corresponding to an interlayer spacing of 3.61 nm. Meanwhile, the diffraction peaks are substantially broader, indicating that the amorphous state of nano-ppy/OMMT is enhanced. This can improve the ionic conductivity and other electrochemical properties of the ionic liquid gel polymer electrolyte [26–28].

Figures 3(a) and 3(b) shows the surface morphologies of MMT and nano-ppy/OMMT by TEM. SEM images of the ILGPE and nano-ppy/OMMT-ILGPE are shown in Figures 3(c) and 3(d). In Figure 3(a), MMT has a particle size, with a diameter of 1-2 $\mu$m. However, the lamellar structure of nano-ppy/OMMT, which has a diameter of approximately 50–100 nm, is evident in Figure 3(b). This provides the basis

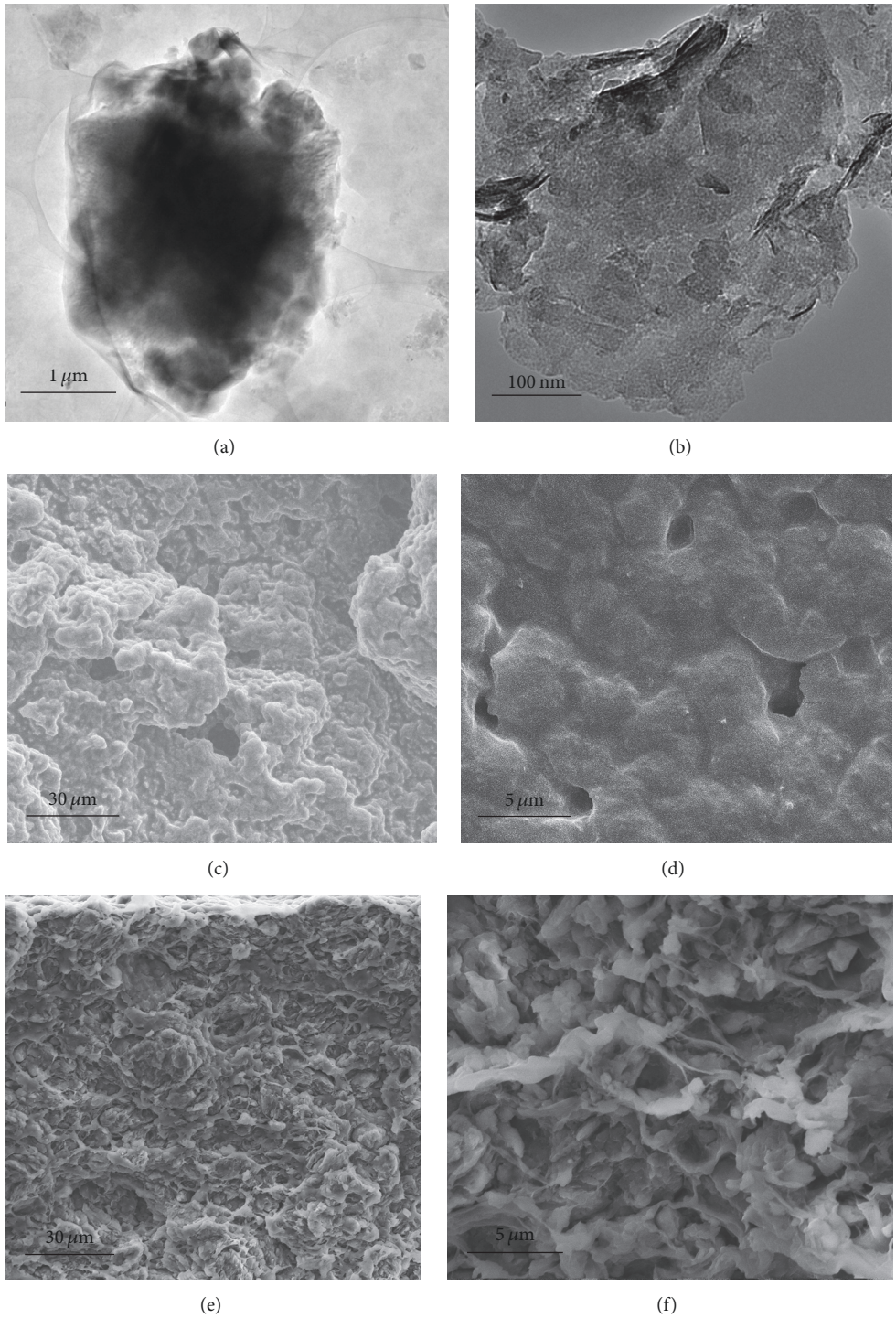


Figure 3: Surface morphology of (a) MMT, (b) nano-ppy/OMMT, (c) ILGPE, (d) nano-ppy/OMMT-ILGPE, (e) the cross-sectional structure of ILGPE, and (f) the cross-sectional structure of nano-ppy/OMMT-ILGPE.

to construct the porous structure of the gel-type composite electrolyte. As shown in Figures 3(c) and 3(e), the sizes of the pores on the ILGPE surface are approximately 5–15 $\mu$m. The sizes and the number of pores are affected by the content and properties of the additive in the casting solution [29, 30]. Figures S2, 3(d), and 3(f) show the porous structure and its diameter of about 1-2 $\mu$m. When nano-ppy/OMMT is added to the composite membrane, the tiny aggregates are formed during the reaction between polymer and nano-ppy/MMT on the surface and cross section of nano-ppy/OMMT-ILGPE. The aggregates can prevent polymer segment from closing and crystallizing. The free volume expands and

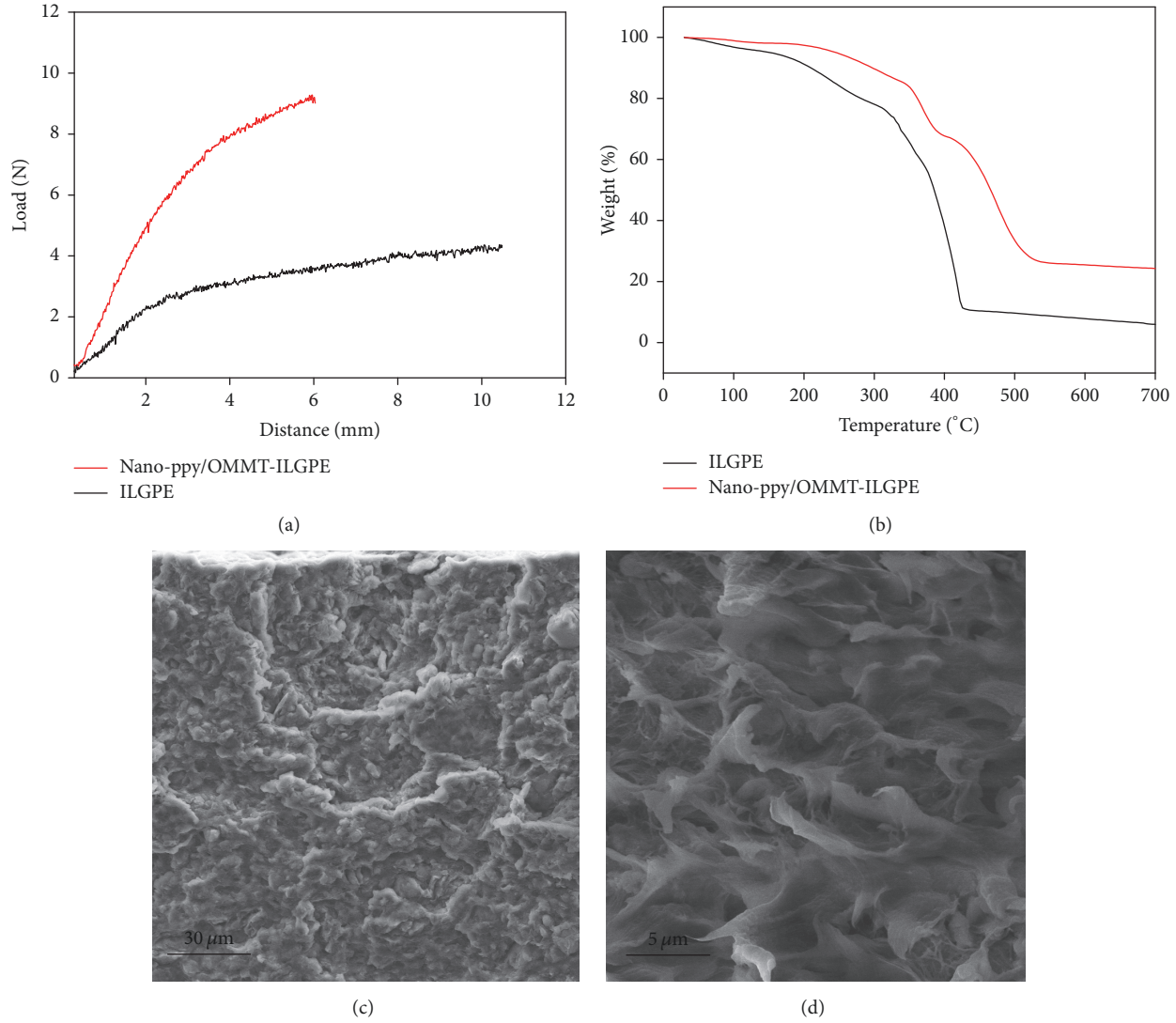


Figure 4: (a) Displacement-load curves of nano-ppy/OMMT-ILGPE and ILGPE; (b) TG curves of nano-ppy/OMMT-ILGPE and ILGPE; (c) the fracture section of ILGPE; (d) the fracture section of nano-ppy/OMMT -ILGPE.

the proportion of amorphous region increases. Meanwhile, many micropores are formed among aggregates, which are staggered and interconnect into the membrane [30]. Thereby, nano-ppy/OMMT can decrease the diameter of pores and create a porous structure. Nano-ppy/OMMT-ILGPE could effectively promote $Li^+$ migration and avoid negative effects on the surface of nano-ppy/OMMT-ILGPE [31]. Thus nano-ppy/OMMT has a significant effect on the average diameter of the pores, which would be beneficial to the migration of $Li^+$ and further enhance the ionic conductivity.

To test the mechanical capacity of nano-ppy/OMMT-ILGPE, the tensile test is used to separately test nano-ppy/OMMT-ILGPE and the ILGPE. The mechanical parameters derived from Figure 4(a) are listed in Table 1. From Table 1, the tensile strength of nano-ppy/OMMT-ILGPE (1.82 MPa) is higher than that of ILGPE (0.88 MPa) without nano-ppy/OMMT. The elongation at sample breakage of nano-ppy/OMMT-ILGPE (5.87 mm) is shorter than that of ILGPE (10.46 mm) without nano-ppy/OMMT. Since there are many large pores in ILGPE, the polymer segment can stretch and shift under the action of external force. When nano-ppy/OMMT is uniformly distributed in the electrolyte membrane, the distance between molecular chains is decreased. The structure of nano-ppy/OMMT-ILGPE gets tighter. When the sample of nano-ppy/OMMT-ILGPE is

Table 1: Tensile properties of nano-ppy/OMMT-ILGPE and ILGPE.

| | Nano-ppy/OMMT-ILGPE | ILGPE |
|---|---|---|
| Maximum load (N) | 9.23 | 4.08 |
| Sectional area ($m^2$) | $5.07 \times 10^{-7}$ | $4.65 \times 10^{-7}$ |
| Tensile strength (MPa) | 1.82 | 0.88 |
| Maximum displacement (mm) | 5.87 | 10.46 |

Table 2: The ionic conductivity ($\sigma$) calculated from Figure 5(a) based on (2).

| Nano-ppy/OMMT (%) | $d$ (cm) | $A$ (cm$^2$) | $R_b$ ($\Omega$) | $\sigma$ (S/cm) |
|---|---|---|---|---|
| 0% | 0.318 | 8.0384 | 436.9 | $9.1 \times 10^{-5}$ |
| 4% | 0.320 | 8.0384 | 82.32 | $4.8 \times 10^{-4}$ |
| 6% | 0.321 | 8.0384 | 63.5 | $6.2 \times 10^{-4}$ |
| 8% | 0.324 | 8.0384 | 33.19 | $1.2 \times 10^{-3}$ |
| 10% | 0.326 | 8.0384 | 76.47 | $5.3 \times 10^{-4}$ |

pulled, nano-ppy/OMMT hinders the extension and mobility of macromolecular chains in Figures 4(c) and 4(d). Therefore, elongation at sample breakage is decreased. In addition, both its tension strength and elasticity modulus are increased. Thus, nano-ppy/OMMT is uniformly distributed in the electrolyte membrane. The mechanical strength of nano-ppy/OMMT-ILGPE can be improved.

It can be seen from Figure 4(b) that ILGPE decomposes in two steps. From 100°C to approximately 300°C, the curves of ILGPE and nano-ppy/OMMT-ILGPE show the evaporation of the NMP solvent. For the curve of ILGPE, the decomposition of both the copolymer and LiTFSI starts at approximately 310°C, and 90% weight loss is detected at 410°C. For the nano-ppy/OMMT-ILGPE, the decomposition of ppy ranges from 350°C to 410°C [32]. The copolymer and LiTFSI of nano-ppy/OMMT-ILGPE begin to decompose at approximately 350°C, and 70% weight loss is detected at 500°C [33, 34]. Because of the addition of nano-ppy/OMMT, the intermolecular force between macromolecular chains and nano-ppy/OMMT is larger than that between individual chains; nano-ppy/OMMT is fully dispersed in the electrolyte membrane. As external heat is transmitted to the inner region of the electrolyte membrane, the layer structure of nano-ppy/OMMT can block the heat transmission. Therefore, ILGPE with nano-ppy/OMMT can delay the evaporation of the NMP solvent and decomposition of the copolymer and LiTFSI. The thermal decomposition temperature of nano-ppy/OMMT-ILGPE is increased, which means that nano-ppy/OMMT-ILGPE has good thermal stability for the preparation of LIBs.

The ionic conductivity of the electrolyte membrane strongly depends on $Li^+$ migration. The AC impedance technique at room temperature reveals that different addition ratios of nano-ppy/OMMT affect the ionic conductivity of nano-ppy/OMMT-ILGPE. Figure 5(a) shows the Nyquist plots of gel polymer electrolyte with different addition ratios of nano-ppy/OMMT, and the values are less than those of ILGPE without nano-ppy/OMMT. Equation (2) is used to calculate the ionic conductivity:

$$\sigma = \frac{d}{R_b \times A}, \tag{2}$$

where $R_b$ is the bulk resistance, $d$ is the film thickness, $A$ is the surface area of the electrode, and $\sigma$ is the ionic conductivity. The results are listed in Table 2.

ILGPE without nano-ppy/OMMT has an ionic conductivity of $9.1 \times 10^{-5}$ S/cm, while the conductivity of the ILGPE reaches $1.2 \times 10^{-3}$ S/cm when the nano-ppy/OMMT reaches 8%. From Figures 5(b) and 5(c), it can be concluded that nano-ppy/OMMT, with its high surface area and layer structure, can inhibit accumulation and crystallization of polymer segments, as well as the closure of pores. More conducting pathways are formed and the ionic transfer ability is enhanced by expanding the free volume, reducing the crystallinity and increasing the amorphous region [31]. By contrast, the ionic conductivity of 10% nano-ppy/OMMT is lower than that of the 8% nano-ppy/OMMT-ILGPE. The former is attributed to the presence of excess nano-ppy/OMMT, and a denser structure of nano-ppy/OMMT-ILGPE is formed, impeding the conducting pathways and retarding ion migration. When 8% nano-ppy/OMMT is added, the ionic conductivity of nano-ppy/OMMT-ILGPE is optimized.

Table 3: The resistance of nano-ppy/OMMT-ILGPE and related data in different temperature.

| $T$ | $\sigma$ (S/cm) | 1000/$T$ (K$^{-1}$) | log $\sigma$ (S/cm) |
|---|---|---|---|
| 20°C | $1.2 \times 10^{-3}$ | 3.41 | −2.92 |
| 30°C | $1.8 \times 10^{-3}$ | 3.30 | −2.74 |
| 40°C | $2.6 \times 10^{-3}$ | 3.19 | −2.59 |
| 50°C | $2.9 \times 10^{-3}$ | 3.10 | −2.54 |
| 60°C | $3.3 \times 10^{-3}$ | 3.00 | −2.48 |
| 70°C | $3.8 \times 10^{-3}$ | 2.92 | −2.42 |
| 80°C | $4.8 \times 10^{-3}$ | 2.83 | −2.31 |

The conductivity of ILGE mainly depends on the migration of the free ions produced in the electrolyte. The lower the apparent activation energy is, the easier the free $Li^+$ migration is. The bulk resistance ($R_b$) of nano-ppy/OMMT-ILGPE is tested by electrochemical impedance spectroscopy (EIS) from 20°C to 80°C. Conductivities ($\sigma$) at different temperatures are obtained according to (2). The detailed parameters are listed in Table 3, and the linear relationship of log $\sigma$ value and 1000/$T$ conforms to Arrhenius conductive behavior presented in Figure 6 [33]. The correlation coefficient $R^2 = 0.96$ of the straight line is obtained:

$$\sigma = \sigma_0 \exp\left[-\frac{E_a}{(RT)}\right], \tag{3}$$

where $E_a$ is apparent activation energy, $T$ is the absolute test temperature, $R$ is the gas constant, and $\sigma$ is the ionic conductivity.

From Figure 6, the fitting result of nano-ppy/OMMT-ILGPE is extracted from the Arrhenius equation; $E_a$ is 30.10 kJ/mol. The apparent activation energy is lower than the values ever reported [33], which is conducive to the free migration of $Li^+$. This demonstrates that nano-ppy/OMMT-ILGPE is good for lithium ion batteries. Meanwhile, the linear relationship of $\sigma$ and temperature conforms to the Vogel-Tamman-Fulcher (VTF). The detailed parameters and fitted curve are exhibited in Table S1 and Figure S3.

Figure 7 displays impedance behavior of ILGPE and nano-ppy/OMMT-ILGPE at room temperature. The bulk resistance ($R_b$) is calculated using a semicircle with a real axis intercept at high frequency. The interfacial resistance ($R_f$)

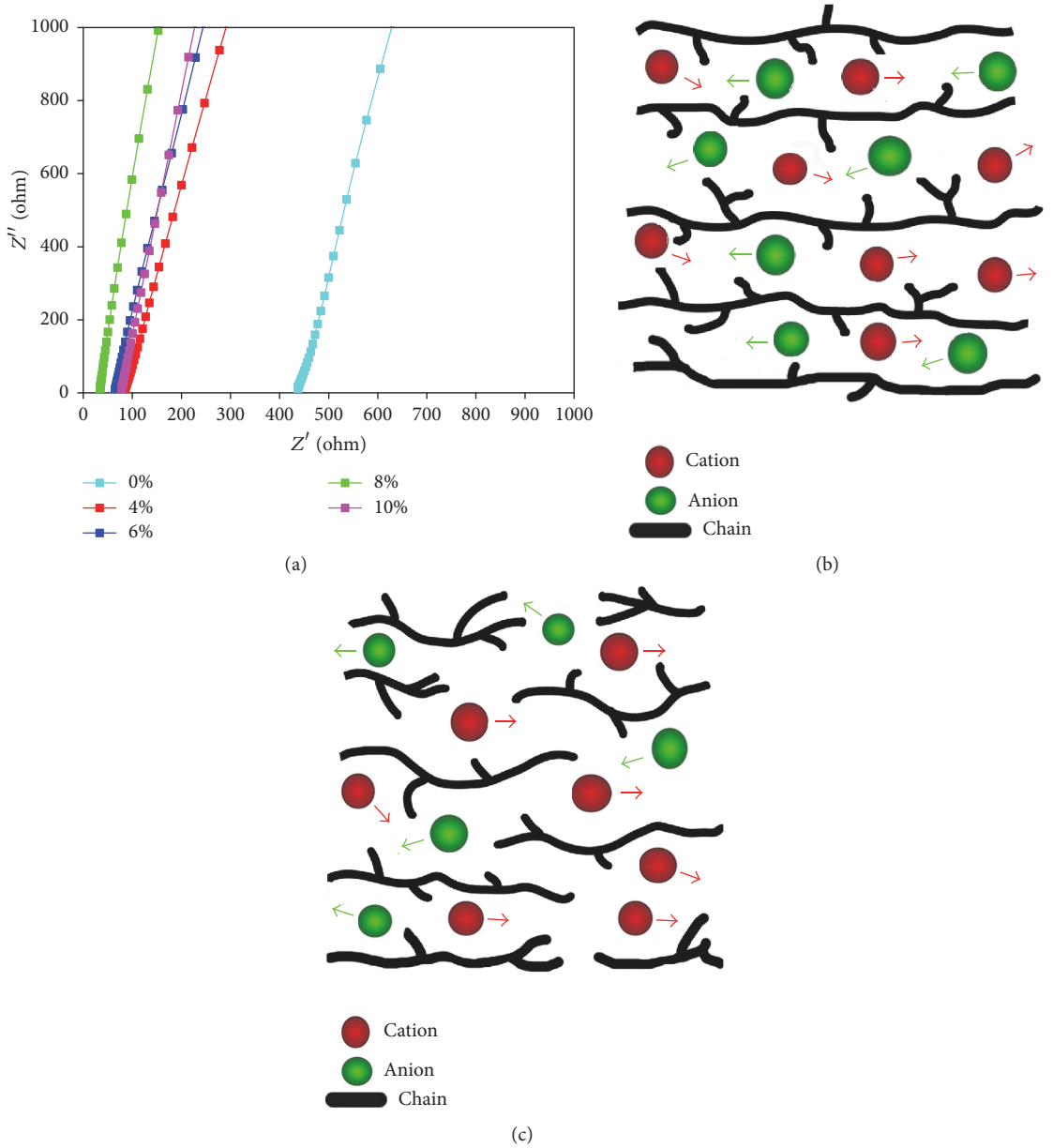


Figure 5: (a) Nyquist plots of gel polymer electrolyte with different addition ratios of nano-ppy/OMMT; (b) schematical representation of ionic conductive process of ILGPE; (c) schematical representation of ionic conductive process of nano-ppy/OMMT-ILGPE.

between the electrode and electrolyte is calculated using the line at low frequency [35, 36]. There is no significant change in $R_b$ before and after the test. However, $R_f$ clearly increased after the test, which may be related to passive film forming between the electrolyte membrane and lithium electrode. The diameter expansion of the $Z'$-$Z''$ semicircles shows an increase in the interface resistance after polarization, thereby restraining the diffusion of lithium ions and the subsequent transfer reaction. The Li-ion transference number ($t_{Li^+}$) represents the charge of the interface resistance before and after polarization and is calculated using (4). The values of the parameters are listed in Table 4.

$$t_{Li^+} = \frac{I_S(\Delta V - I_0 R_0)}{I_0(\Delta V - I_S R_S)}, \quad (4)$$

Table 4: The transference number ($t_{Li^+}$) calculated from Figure 6 based on (4).

| | $R_0$ | $R_S$ | $I_0$ | $I_S$ | $t_{Li^+}$ |
|---|---|---|---|---|---|
| ILGPE | 1001.8 | 1372.57 | $2.11 \times 10^{-6}$ | $8.16 \times 10^{-7}$ | 0.34 |
| Nano-ppy/OMMT-ILGPE | 520 | 884.82 | $1.52 \times 10^{-6}$ | $1.08 \times 10^{-6}$ | 0.72 |

where $I_0$ and $I_S$ are initial and steady-state current values, $\Delta V$ is the applied potential difference (10 mV), and $R_0$ and $R_S$ are the initial interfacial resistance and steady-state interfacial resistance, respectively.

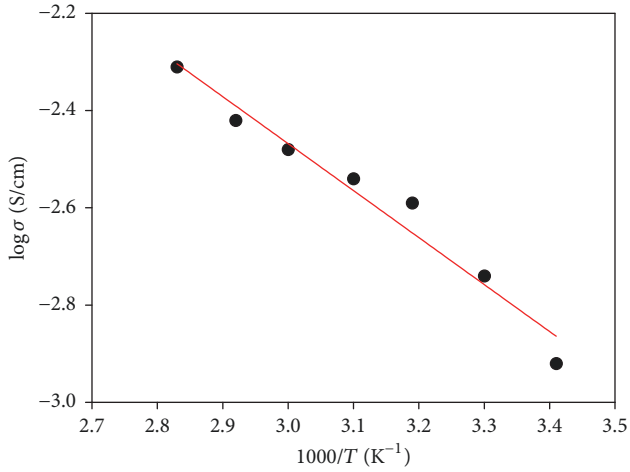


Figure 6: Arrhenius equation fitting curve of nano-ppy/OMMT-ILGPE.

In Figure 7 and Table 4, when nano-ppy/OMMT is doped into ILGPE, the 1-2 $\mu$m pores appear on the surface which stagger and interconnect into the membrane in Figure 3(f). The porous structure of nano-ppy/OMMT-ILGPE can get a high surface area. In some way, the Li-ion intercalation and deintercalation abilities are increased, and the transfer resistance of nano-ppy/OMMT-ILGPE is decreased [31]. The Li-ion transport of nano-ppy/OMMT-ILGPE is effectively improved. The porous structure of nano-ppy/OMMT-ILGPE increases $t_{Li^+}$ up to 0.72, which is approximately twice that of ILGPE without nano-ppy/OMMT. Therefore, nano-ppy/OMMT-ILGPE can contribute to the improvement of Li-ion transport in the LIBs.

In Figure 8(a), the reduction peak and oxidation peak appear at 3.4 V and 4.2 V in the 1st cycle, respectively. The cathodic peak shifts to a lower potential in the 2nd cycle, which indicates that a passive film is formed between the electrolyte membrane and cathode material during the 1st cycle [37]. After activation and formation of the passive film in the 1st cycle, the reduction peak shifts to 3.25 V, which could be ascribed to the diffusive phenomena between the cathode and membrane during the 2nd cycle. The peak positions are invariable in the 3rd and 4th cycles. In the following cycles, nano-ppy/OMMT-ILGPE exhibits better compatibility, stability, and reversibility.

In Figure 8(b), the 1st charge/discharge capacity of the Li|nano-ppy/OMMT-ILGPE|$LiNi_{1/3}Co_{1/3}Mn_{1/3}O_2$ cell is 144.8 mAh/g/121.3 mAh/g (0.5 C) and the coulombic efficiency is 83.8% (0.5 C). In the 2nd charge and discharge cycle, the specific capacity of the cell rises [38]. After 100 cycles, the discharge performance of the Li|nano-ppy/OMMT-ILGPE|$LiNi_{1/3}Co_{1/3}Mn_{1/3}O_2$ cell is 124.5 mAh/g (0.5 C) and the coulombic efficiency is quite close to 100% (0.5 C). However, comparing ILGPE with nano-ppy/OMMT-LGPE (see Figure 8(c)), the 1st charge/discharge capacity of the Li|ILGPE|$LiNi_{1/3}Co_{1/3}Mn_{1/3}O_2$ cell is 143.1 mAh/g/107.4 mAh/g (0.5 C) and the coulombic efficiency is 74.8% (0.5 C). After 100 cycles, the discharge performance of the Li|ILGPE|$LiNi_{1/3}Co_{1/3}Mn_{1/3}O_2$ cell is 105.8 mAh/g (0.5 C). The charge/discharge performance and the coulombic efficiency of ILGPE are less than those of nano-ppy/OMMT-ILGPE for the charge and discharge processes, which indicates that nano-ppy/OMMT could restrain negative effects between the electrode and impurities so that the thickness of the passive film is reduced [13, 39]. Therefore, the specific capacity and coulombic efficiency of the cell with nano-ppy/OMMT-ILGPE are better than those of the cell with the ILGPE.

To confirm the difference in the thicknesses of the passive films on the surfaces of nano-ppy/OMMT-ILGPE and ILGPE subjected to charge and discharge tests at room temperature, the EIS values of the cells before and after 100 cycles at 0.5 C are shown in Figures 8(d) and 8(e). In Figure 8(d), the bulk resistance ($R_b$) and charge transfer resistance ($R_{ct}$) of the cell assembled with nano-ppy/OMMT-ILGPE are smaller than those of the cell with ILGPE before 100 cycles because the porous structure of the electrolyte membrane is improved when nano-ppy/OMMT is doped into ILGPE. The porous structure of nano-ppy/OMMT-ILGPE with a high surface area can absorb more electrolyte and form more conducting pathways, thus improving the ability of lithium to migrate. Therefore, the porous structure of nano-ppy/OMMT-ILGPE can reduce the $R_b$ and $R_{ct}$ of nano-ppy/OMMT-ILGPE. After 100 cycles, nano-ppy/OMMT-ILGPE and ILGPE present two separate semicircles at the high and low frequencies, which are caused by the solid electrolyte interface resistance ($R_{SEI}$) and $R_{ct}$ (see Figure 8(e)) [40]. Compared with the $R_{SEI}$ of ILGPE, the $R_{SEI}$ of nano-ppy/OMMT-ILGPE is significantly low because nano-ppy/OMMT reacts with impurities to inhibit any negative effects between the surfaces of the electrode and membrane. The Li-ion deintercalation ability increases, which could reduce $\sigma$ and make the passive film thinner [41]. $R_{ct}$ of the nano-ppy/OMMT-ILGPE is substantially smaller than that of ILGPE because the improved porous structure of nano-ppy/OMMT-ILGPE increases the Li-ion deintercalation ability and reduces $R_{ct}$ to some extent. This reveals that the porous structure of nano-ppy/OMMT-ILGPE is beneficial to the increase of the transfer ability of lithium ions and to the improvement of the cycle stability of the lithium ion battery.

To confirm the electrochemistry performance of nano-ppy/OMMT-ILGPE, the reversible discharge capabilities of the cells with nano-ppy/OMMT-ILGPE and ILGPE at different C-rates are evaluated, as shown in Figure 8(f). The testing voltage is between 2.7 V and 4.2 V, and the charge/discharge current density ranges from 0.2 C to 2 C. The reversible discharge capacities of the cells with nano-ppy/OMMT-ILGPE and ILGPE are 129.1 and 120.1 mAh/g (0.2 C), 114.6 and 103.5 mAh/g (0.5 C), 106.3 and 88.9 mAh/g (1 C), and 96.2 and 71.3 mAh/g (2 C), respectively. The reversible discharge capacity gradually decreases, while the current density increases. The differences between the electrolyte membranes become more evident at the higher current densities. The reversible discharge capacity of the cell with nano-ppy/OMMT-ILGPE is 96.2 mAh/g (2 C), meaning that the discharge performance of nano-ppy/OMMT-ILGPE is better at a high current density. When the current density is further

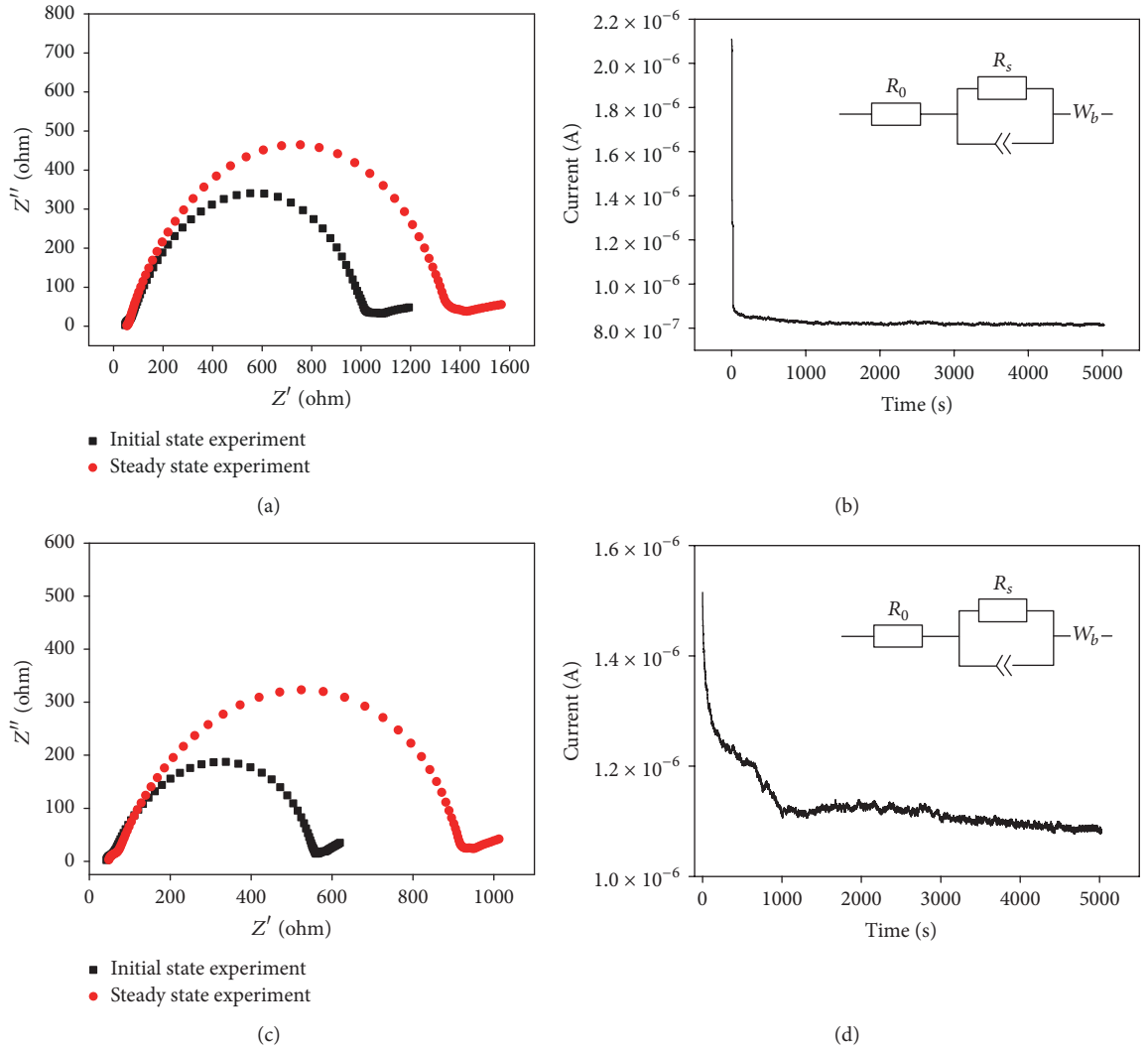


Figure 7: (a) AC impedance of ILGPE, (b) chronoamperometry of ILGPE, (c) AC impedance of nano-ppy/OMMT-ILGPE, (d) chronoamperometry of nano-ppy/OMMT-ILGPE.

decreased to 0.2 C, the reversible discharge capacity of the cell with nano-ppy/OMMT-ILGPE is 118.7 mAh/g. However, the reversible discharge capacity of the cell with ILGPE is 91.6 mAh/g. It is found that the discharge performance of the cell with ILGPE is optimized after the addition of nano-ppy/OMMT [42].

## 4. Conclusions

Nano-ppy/OMMT is prepared in situ during the polymerization reaction of the py monomers between the molecular layers of MMT. The diameter of nano-ppy/OMMT is approximately 50–100 nm, and it has a flake structure and large interlayer spacing. Nano-ppy/OMMT is considered to be a good inorganic doping agent for the preparation of a composite gel polymer electrolyte with a porous structure. Nano-ppy/OMMT-ILGPE has a porous structure with an approximately 1-2 $\mu$m aperture, relatively high transference number of lithium ion (0.72), and high conductivity ($1.2 \times 10^{-3}$ S/cm) at room temperature. The good electrochemical stability of nano-ppy/OMMT-ILGPE is favourable for use in $Li/LiNi_{1/3}Co_{1/3}Mn_{1/3}O_2$ cells. Nano-ppy/OMMT-ILGPE exhibits better charge/discharge cycling at 0.5 C and is superior to ILGPE in specific capacity and cycle stability. Therefore, nano-ppy/OMMT-ILGPE has many advantages, such as good thermal stability, mechanical performance, and environmental friendliness, as well as a high energy density and cycling stability, and can be used as an ideal gel polymer electrolyte material for lithium ion batteries.

## Conflicts of Interest

The authors declare that they have no conflicts of interest.

## Supplementary Materials

Figure S1: mechanism of oxidative chemical polymerization of ppy. Figure S2: the microstructures of (a) ILGPE and

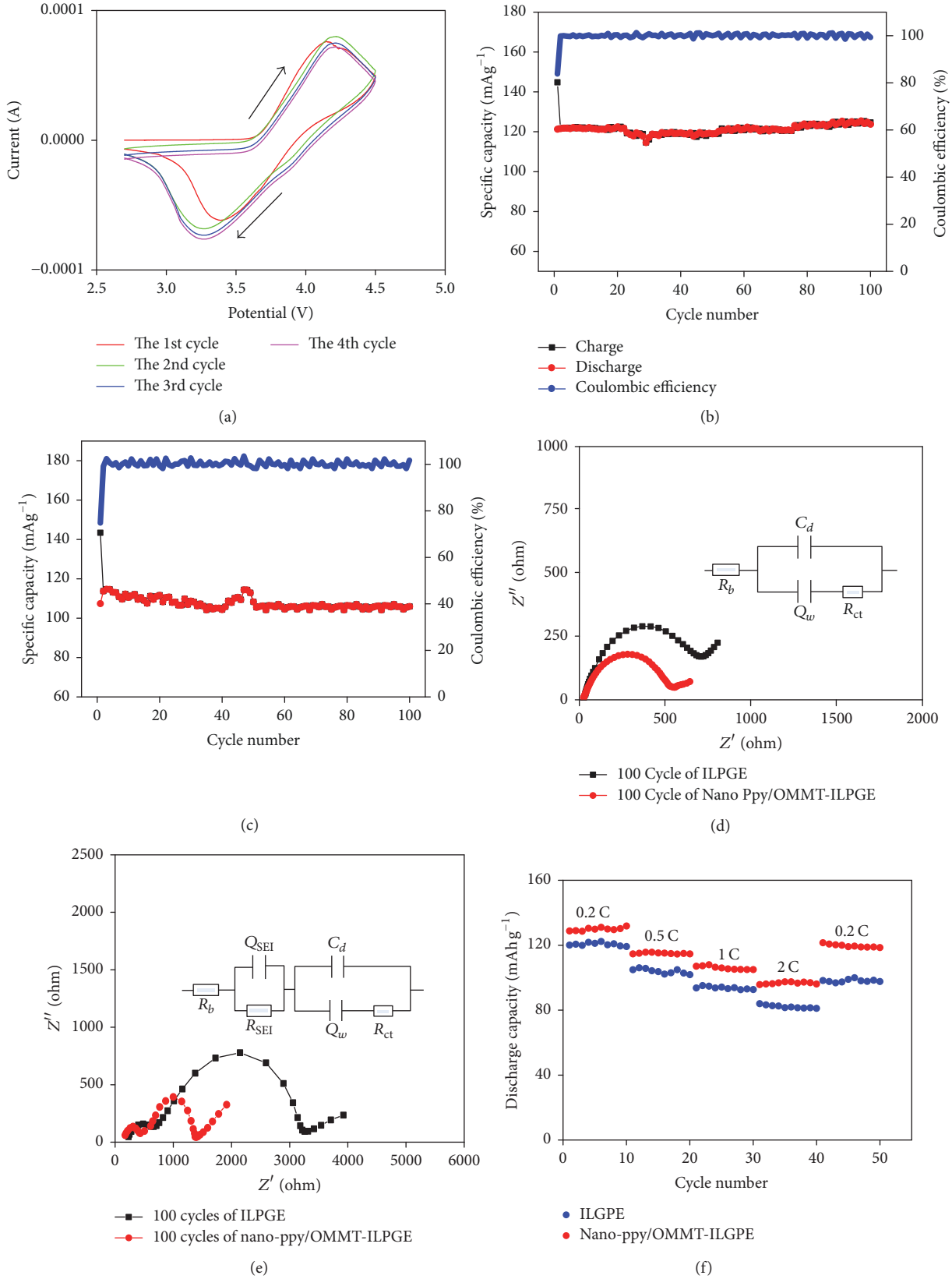


Figure 8: (a) Cyclic voltammetry curves of Li|nano-ppy/OMMT-ILGPE|$LiNi_{1/3}Co_{1/3}Mn_{1/3}O_2$ cell at a scan rate of 0.1 mV/s and the potential between 2.7 V and 4.5 V. (b) The charge/discharge curve of Li|nano-ppy/OMMT-ILGPE|$LiNi_{1/3}Co_{1/3}Mn_{1/3}O_2$ cell at 0.5 C. (c) The charge/discharge curve of Li|ILGPE|$LiNi_{1/3}Co_{1/3}Mn_{1/3}O_2$ cell at 0.5 C. (d) EIS spectrum of cell before the 100 cycles. (e) EIS spectrum of cell after the 100 cycles. (f) Electrochemical performance of ILGPE and nano-ppy/OMMT-ILGPE at variable discharge current density tests between 0.2 C and 2 C.

(b) nano-ppy/OMMT-ILGPE at the same magnification. Table S1: conductivities ($\sigma$) of nano-ppy/OMMT-ILGPE at different temperatures. Figure S3: VTF fitting curve of nano-ppy/OMMT-ILGPE. *(Supplementary Materials)*

## References


[1] G. A. Elia, R. Bernhard, and J. Hassoun, "A lithium-ion oxygen battery using a polyethylene glyme electrolyte mixed with an ionic liquid," *RSC Advances*, vol. 5, no. 27, pp. 21360–21365, 2015.

[2] Y. S. Yun, S.-W. Song, S.-Y. Lee, S.-H. Kim, and D.-W. Kim, "Lithium metal polymer cells assembled with gel polymer electrolytes containing ionic liquid," *Current Applied Physics*, vol. 10, no. 4, pp. e97–e100, 2010.

[3] J. Krummacher, S. Passerini, and A. Balducci, "Ionic liquid assisted solid-state synthesis of lithium iron oxide nanoparticles for rechargeable lithium ion batteries," *Solid State Ionics*, vol. 280, pp. 37–43, 2015.

[4] R. L. Lavall, S. Ferrari, C. Tomasi et al., "Novel polymer electrolytes based on thermoplastic polyurethane and ionic liquid/lithium bis(trifluoromethanesulfonyl)imide/propylene carbonate salt system," *Journal of Power Sources*, vol. 195, no. 17, pp. 5761–5767, 2010.

[5] P. Raghavan, X. Zhao, C. Shin et al., "Preparation and electrochemical characterization of polymer electrolytes based on electrospun poly(vinylidene fluoride-co-hexafluoropropylene)/polyacrylonitrile blend/composite membranes for lithium batteries," *Journal of Power Sources*, vol. 195, no. 18, pp. 6088–6094, 2010.

[6] H. Lee, M. Yanilmaz, O. Toprakci, K. Fu, and X. Zhang, "A review of recent developments in membrane separators for rechargeable lithium-ion batteries," *Energy & Environmental Science*, vol. 7, no. 12, pp. 3857–3886, 2014.

[7] C. M. Costa, J. Nunes-Pereira, V. Sencadas, M. M. Silva, and S. Lanceros-Méndez, "Effect of fiber orientation in gelled poly(vinylidene fluoride) electrospun membranes for Li-ion battery applications," *Journal of Materials Science*, vol. 48, no. 19, pp. 6833–6840, 2013.

[8] S. Grandi, P. Mustarelli, A. Carollo, C. Tomasi, E. Quartarone, and A. Magistris, "PWA Doped SiO2 PEG Hybrid Materials of Class II," *Materials Sciences and Applications*, vol. 01, no. 05, pp. 285–291, 2010.

[9] B. Yu, F. Zhou, C. Wang, and W. Liu, "A novel gel polymer electrolyte based on poly ionic liquid 1-ethyl 3-(2-methacryloyloxy ethyl) imidazolium iodide," *European Polymer Journal*, vol. 43, no. 6, pp. 2699–2707, 2007.

[10] A. Manuel Stephan and K. S. Nahm, "Review on composite polymer electrolytes for lithium batteries," *Polymer Journal*, vol. 47, no. 16, pp. 5952–5964, 2006.

[11] M. Kaur, S. Singh, and R. Mehta, "Physico-chemical modification induced in PLGA/OMMT nanocomposite films by Li3+ ion beam," *Vacuum*, vol. 125, pp. 170–179, 2016.

[12] M. Deka and A. Kumar, "Electrical and electrochemical studies of poly(vinylidene fluoride)-clay nanocomposite gel polymer electrolytes for Li-ion batteries," *Journal of Power Sources*, vol. 196, no. 3, pp. 1358–1364, 2011.

[13] Q. Zhang, F. Ding, W. Sun, and L. Sang, "Preparation of LAGP/P(VDF-HFP) polymer electrolytes for Li-ion batteries," *RSC Advances*, vol. 5, no. 80, pp. 65395–65401, 2015.

[14] J.-W. Kim, K.-S. Ji, J.-P. Lee, and J.-W. Park, "Electrochemical characteristics of two types of PEO-based composite electrolyte with functional SiO2," *Journal of Power Sources*, vol. 119-121, pp. 415–421, 2003.

[15] N. Byrne, J. Efthimiadis, D. R. MacFarlane, and M. Forsyth, "The enhancement of lithium ion dissociation in polyelectrolyte gels on the addition of ceramic nano-fillers," *Journal of Materials Chemistry*, vol. 14, no. 1, pp. 127–133, 2004.

[16] F. Croce, S. Sacchetti, and B. Scrosati, "Advanced, high-performance composite polymer electrolytes for lithium batteries," *Journal of Power Sources*, vol. 161, no. 1, pp. 560–564, 2006.

[17] M. Yoonessi, H. Toghiani, W. L. Kingery, and C. U. Pittman Jr., "Preparation, characterization, and properties of exfoliated/delaminated organically modified clay/dicyclopentadiene resin nanocomposites," *Macromolecules* , vol. 37, no. 7, pp. 2511–2518, 2004.

[18] I. Kelnar, J. Kratochvíl, I. Fortelný et al., "Effect of halloysite on structure and properties of melt-drawn PCL/PLA microfibrillar composites," *Express Polymer Letters*, vol. 10, no. 5, pp. 381–393, 2016.

[19] L. T. Costa, R. L. Lavall, R. S. Borges, J. Rieumont, G. G. Silva, and M. C. C. Ribeiro, "Polymer electrolytes based on poly(ethylene glycol) dimethyl ether and the ionic liquid 1-butyl-3-methylimidazolium hexafluorophosphate: Preparation, physico-chemical characterization, and theoretical study," *Electrochimica Acta*, vol. 53, no. 4, pp. 1568–1574, 2007.

[20] D. Bansal, F. Cassel, F. Croce, M. Hendrickson, E. Plichta, and M. Salomon, "Conductivities and transport properties of gelled electrolytes with and without an ionic liquid for Li and Li-Ion batteries," *The Journal of Physical Chemistry B*, vol. 109, no. 10, pp. 4492–4496, 2005.

[21] B. Singh and S. S. Sekhon, "Polymer electrolytes based on room temperature ionic liquid: 2,3-dimethyl-l-octylimidazolium triflate," *The Journal of Physical Chemistry B*, vol. 109, no. 34, pp. 16539–16543, 2005.

[22] A. Pattanayak and S. C. Jana, "Properties of bulk-polymerized thermoplastic polyurethane nanocomposites," *Polymer Journal*, vol. 46, no. 10, pp. 3394–3406, 2005.

[23] S. Mou, Y. Lu, and Y. Jiang, "A facile and cheap coating method to prepare SiO2/melamine-formaldehyde and SiO2/urea-formaldehyde composite microspheres," *Applied Surface Science*, vol. 384, pp. 258–262, 2016.

[24] J. Wang, Y. Xu, F. Yan, J. Zhu, and J. Wang, "Template-free prepared micro/nanostructured polypyrrole with ultrafast charging/discharging rate and long cycle life," *Journal of Power Sources*, vol. 196, no. 4, pp. 2373–2379, 2011.

[25] B. K. Price, J. L. Hudson, and J. M. Tour, "Green chemical functionalization of single-walled carbon nanotubes in ionic liquids," *Journal of the American Chemical Society*, vol. 127, no. 42, pp. 14867–14870, 2005.

[26] C.-Y. Chiang, Y. J. Shen, M. J. Reddy, and P. P. Chu, "Complexation of poly(vinylidene fluoride):LiPF6 solid polymer electrolyte with enhanced ion conduction in 'wet' form," *Journal of Power Sources*, vol. 123, no. 2, pp. 222–229, 2003.

[27] Y. Song, Z. Zhao, W. Yu, B. Li, and X. Chen, "Morphological structures of poly(vinylidene fluoride)/montmorillonite nanocomposites," *SCIENCE CHINA Chemistry*, vol. 50, no. 6, pp. 790–796, 2007.

[28] C. Fang, S. Yang, X. Zhao, P. Du, and J. Xiong, "Electrospun montmorillonite modified poly(vinylidene fluoride) nanocomposite separators for lithium-ion batteries," *Materials Research Bulletin*, vol. 79, pp. 1–7, 2016.

[29] K. M. Kim, N.-G. Park, K. S. Ryu, and S. H. Chang, "Characterization of poly(vinylidenefluoride-co-hexafluoropropylene)based polymer electrolyte filled with Tio2 nanoparticles," *Polymer Journal*, vol. 43, no. 14, pp. 3951–3957, 2002.

[30] K. M. Kim, N.-G. Park, K. S. Ryu, and S. H. Chang, "Characteristics of PVdF-HFP/TiO2 composite membrane electrolytes prepared by phase inversion and conventional casting methods," *Electrochimica Acta*, vol. 51, no. 26, pp. 5636–5644, 2006.

[31] Y. Ma, L. B. Li, G. X. Gao, X. Y. Yang, and Y. You, "Effect of montmorillonite on the ionic conductivity and electrochemical properties of a composite solid polymer electrolyte based on polyvinylidenedifluoride/polyvinyl alcohol matrix for lithium ion batteries," *Electrochimica Acta*, vol. 187, pp. 535–542, 2016.

[32] J. Cao, G. Hu, Z. Peng, K. Du, and Y. Cao, "Polypyrrole-coated LiCoO2 nanocomposite with enhanced electrochemical properties at high voltage for lithium-ion batteries," *Journal of Power Sources*, vol. 281, pp. 49–55, 2015.

[33] L. Li, Y. Ma, W. Wang, Y. Xu, J. You, and Y. Zhang, "A thermal and electrochemical properties research on gel polymer electrolyte membrane of lithium ion battery," *Journal of Physics and Chemistry of Solids*, vol. 99, pp. 159–166, 2016.

[34] L. Li, J. Wang, P. Yang et al., "Preparation and characterization of gel polymer electrolytes containing N-butyl-N-methylpyrrolidinium bis(trifluoromethanesulfonyl) imide ionic liquid for lithium ion batteries," *Electrochimica Acta*, vol. 88, pp. 147–156, 2013.

[35] W. Cho, S.-M. Kim, J. H. Song et al., "Improved electrochemical and thermal properties of nickel rich $LiNi_{0.6}Co_{0.2}Mn_{0.2}O_2$ cathode materials by $SiO_2$ coating," *Journal of Power Sources*, vol. 282, pp. 45–50, 2015.

[36] X. Xu, H. Zhang, Y. Chen, N. Li, Y. Li, and L. Liu, "SiO2@SnO2/graphene composite with a coating and hierarchical structure as high performance anode material for lithium ion battery," *Journal of Alloys and Compounds*, vol. 677, pp. 237–244, 2016.

[37] J. Jin, Z. Wen, X. Liang, Y. Cui, and X. Wu, "Gel polymer electrolyte with ionic liquid for high performance lithium sulfur battery," *Solid State Ionics*, vol. 225, pp. 604–607, 2012.

[38] L. Liu, P. Yang, L. Li, Y. Cui, and M. An, "Application of bis(trifluoromethanesulfonyl)imide lithium-N-methyl-N- butylpiperidinium-bis(trifluoromethanesulfonyl)imide-poly(vinylidene difluoride-co-hexafluoropropylene) ionic liquid gel polymer electrolytes in Li/LiFePO4 batteries at different temperatures," *Electrochimica Acta*, vol. 85, pp. 49–56, 2012.

[39] Y. Zhang, Z. Wang, H. Xiang, P. Shi, and H. Wang, "A thin inorganic composite separator for lithium-ion batteries," *Journal of Membrane Science*, vol. 509, pp. 19–26, 2016.

[40] T. Yang, L. Sang, F. Ding, J. Zhang, and X. Liu, "Three- and four-electrode EIS analysis of water stable lithium electrode with solid electrolyte plate," *Electrochimica Acta*, vol. 81, pp. 179–185, 2012.

[41] J. Cao, L. Wang, X. He et al., "In situ prepared nano-crystalline TiO2-poly(methyl methacrylate) hybrid enhanced composite polymer electrolyte for Li-ion batteries," *Journal of Materials Chemistry A*, vol. 1, no. 19, pp. 5955–5961, 2013.

[42] J. Lee, C.-L. Lee, K. Park, and I.-D. Kim, "Synthesis of an Al2O3-coated polyimide nanofiber mat and its electrochemical characteristics as a separator for lithium ion batteries," *Journal of Power Sources*, vol. 248, pp. 1211–1217, 2014.